A Study of Cross-Bridge Kelvin Resistor Structures for Reliable Measurement of Low Contact Resistances

N. Stavitski[1], *Student Member, IEEE*, J.H. Klootwijk[2], *Member, IEEE*
H.W. van Zeijl[3], A.Y. Kovalgin[1], R.A.M. Wolters[1,4]

[1] MESA+ Institute for Nanotechnology, Chair of Semiconductor Components
University of Twente, Postbox 217, 7500AE Enschede, The Netherlands
E-mail: n.stavitski@utwente.nl
[2] Philips Research, High Tech Campus 4, 5656 AE Eindhoven, The Netherlands
[3] DIMES, Delft University of Technology, Feldmannweg 17, 2628 CT Delft, The Netherlands
[4] NXP Research Eindhoven, High Tech Campus 4, 5656 AE Eindhoven, The Netherlands

ABSTRACT

The parasitic factors that strongly influence the measurement accuracy of Cross-Bridge Kelvin Resistor (CBKR) structures for low specific contact resistances (ρ_c) have been extensively discussed during last few decades and the minimum of the ρ_c value, which could be accurately extracted, was estimated. We fabricated a set of various metal-to-metal CBKR structures with different geometries, i.e., shapes and dimensions, to confirm this limit experimentally. As a result, a model was developed to account for the actual current flow and a method for reliable ρ_c extraction was created. It was found that in our case of metal-to-metal contacts, the measured CBKR contact resistance was determined by the dimensions of the two-metal stack in the area of contact and sheet resistances of the metals used.

INTRODUCTION

Cross-Bridge Kelvin Resistor (CBKR) structures are the most widely used test structures to characterize metal-semiconductor contacts in the planar devices of VLSI technology [1, 2]. On the other hand, CBKR was found to be very sensitive to lateral current crowding around the contact when the contact window is smaller than the underlying layer. Several simulations and correction methods were introduced in order to account for this current crowding effect [3-6]. However in the low resistance range, the extracted silicide-to-silicon specific contact resistance (ρ_c) values, obtained using CBKR structures, were still orders of magnitude different from the results obtained using other methods [2]. An explanation of this phenomenon is the accuracy problems during the data extraction using CBKR structures in the range of ~ 10^{-8} $\Omega \cdot cm^2$ and below [7]. In this case, the lateral current flow around the contacts gives rise to an even higher additional resistance [8, 9]. This effect becomes more pronounced for a lower ρ_c and a higher sheet resistance (R_{sh}) of the underlying layer. Simulations show that for $\rho_c < 10^{-7}$ $\Omega \cdot cm^2$ the extracted ρ_c can differ by one or two orders of magnitude from the actual value [6]. Moreover, the trend in the modern technology of high-density integrated circuits is toward lower ρ_c and higher R_{sh} values, due to the shallower junctions. This will further complicate the interpretation of CBKR measurement results.

Our research is therefore concerned with finding the minimum contact resistance, which can be obtained experimentally using CBKR test structures, and developing a correction model to account for the actual current flow. For that purpose, CBKR structures of different geometries, i.e., dimensions and shapes of the contact area were designed and manufactured. These structures were evaluated for metal-to-metal contacts to assure the case of very low contact resistances.

MEASUREMENT TECHNIQUE AND TEST STRUCTURES DESCRIPTION

A standard four-terminal CBKR test structure is used to determine ρ_c of metal-to-metal contacts (Fig. 1).

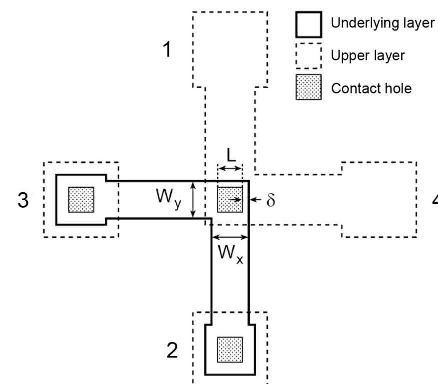

Fig. 1. Four-terminal CBKR structure with geometry parameters definition. In our structures, the contact geometry parameters (δ and *L)* for both layers are identical, unless mentioned otherwise.

The measurement principle consists of forcing the current (I) between contacts 1 and 2 and measuring the voltage drop (V_{34}) between contacts 3 and 4. The actually measured Kelvin resistance R_k can then be found as

$$R_k = \frac{V_{34}}{I}. \quad (1)$$

In the 1D-Model approach [4], the specific contact resistance can be calculated directly from the contact area A and R_k, assuming that the resistance due to the voltage drop across the actual contact (R_c) equals R_k:

$$\rho_c = R_c A = R_k A. \quad (2)$$

The 1D-Model does not account for the current flowing in the overlap region (δ) of the underlying layer (Fig. 1), when $\delta > 0$. In that case the so-called 2D-Model should be applied [4]. The analytical model by Schreyer and Saraswat was used in this study as a starting point for the correction. The measured R_k is then a sum of the R_c and the resistance due to the current flow around the contact in the overlap region (R_{geom}) (3). The ρ_c can further be extracted from (4), where R_{sh} is the sheet resistance of the underlying layer. The contact geometry parameters are defined in Fig. 1.

$$R_k = R_c + R_{geom} \quad (3)$$

$$R_k = \frac{\rho_c}{A} + \frac{4R_{sh}\delta^2}{3W_x W_y}\left[1 + \frac{\delta}{2(W_x - \delta)}\right] \quad (4)$$

In order to verify the validity of the results obtained, the CBKR structures were designed to cover a wide range of contact sizes (i.e., length L for square contacts and diameter D for round contacts) and δ. Some of the structures were designed with two δ, different for the back and front metal layers: δ_B and δ_F, respectively. To exclude the uncertainty in the definition of δ in the case of round contacts, the metal tap width (V_{tap}, Fig. 2) was varied as well. The details are summarized in Table I. An example of the square and round CBKR structure is presented in Fig. 2.

TABLE I
IMPORTANT GEOMETRY PARAMETERS OF OUR CBKR STRUCTURES

Geometry	L (D) µm	δ µm	δ_F µm	δ_B µm	V_{TAP} µm
Square	1	0.2 – 5	n/a	n/a	n/a
Square	2	0.2 – 5	n/a	n/a	n/a
Square	4.4	0.2 – 5	n/a	n/a	n/a
Square	8.9	0.2 – 5	n/a	n/a	n/a
Square	17.7	0.2 – 5	n/a	n/a	n/a
Square	8.9	n/a	0.2 – 5	0.2 – 5	n/a
Round	5	0.5 – 10	n/a	n/a	1 – 2
Round	10	0.5 – 10	n/a	n/a	1 – 2
Round	20	0.5 – 10	n/a	n/a	1 – 2
Round	10	n/a	1 – 5	1 – 5	2
Round	20	n/a	1 – 5	1 – 5	2

TEST STRUCTURES FABRICATION

The (100) p-type Si wafers with a 1 µm-thick thermal oxide were used to fabricate the test structures for this study. First, a 0.675 or 1.4 µm- thick Al layer was sputtered and patterned using I-line lithography and plasma etching. Then, a 0.8 µm-thick layer of SiO_2 was deposited by PECVD and the contact holes were opened. Prior to the second Al deposition, the contacts were in-situ RF-precleaned. The second Al layer of 0.675 or 1.41 µm was sputtered and patterned as the front metallization layer, including the bond pads. Finally, the structures received 20-min annealing at 400 °C in a N_2/H_2 (10%) mixture.

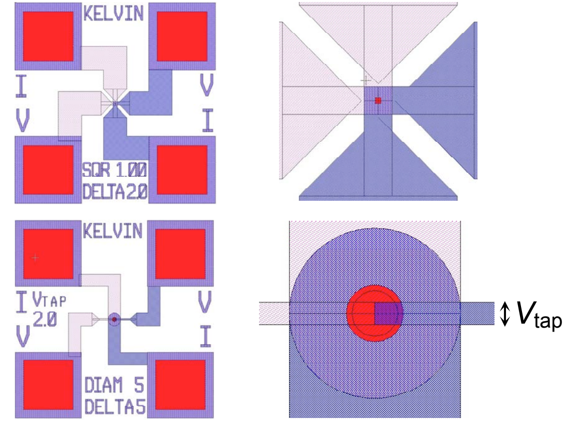

Fig. 2. An example of the newly-designed square and round CBKR structures. The complete structure including the bond pads is on the left- and a blow up of the actual contact is on the right-hand side.

RESULTS AND DISCUSSION

A. Measured Kelvin resistance R_k for square contacts with symmetric δ for back and front metals

The R_k data as a function of contact size $A = L^2$ and the overlap size δ are given in Fig. 3 and Fig. 4, respectively. It can clearly be seen that R_k increases with increasing δ and decreases with increasing contact size. This is in agreement with the theory (4), demonstrating, that for $\delta > 0$, the lateral current flow gives rise to an additional voltage drop that is included in V_{34}, leading to a higher R_k value.

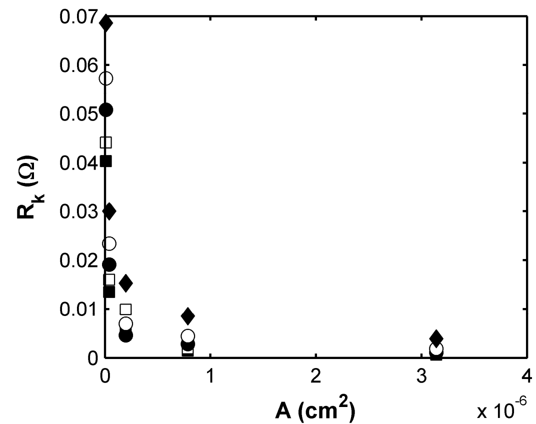

Fig. 3. Measured Kelvin resistance vs. contact size for given symmetric overlap area sizes for square contacts: δ = 0.2 µm (■), δ = 0.5 µm (□), δ = 1 µm (●), δ = 2 µm (○), δ = 5 µm (◆).

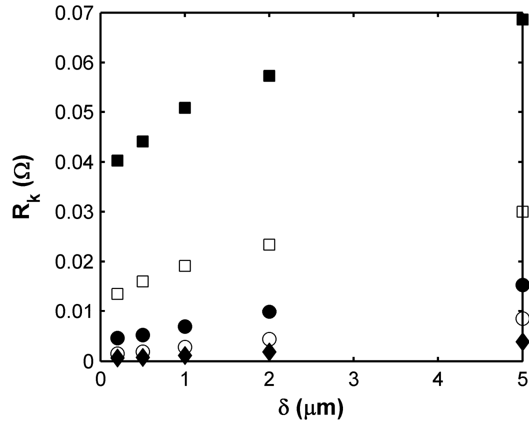

Fig. 4. Measured Kelvin resistance vs. symmetric overlap size for given square contact sizes: L = 1 µm (■), L = 2 µm (□), L = 4.4 µm (●), L = 8.9 µm (○), L = 17.7 µm (◆).

B. Measured Kelvin resistance R_k for square contacts with non-symmetric overlap areas for back and front metals

As expected for the non-symmetric overlaps for front and back metals, the R_k values were dependent on the direction of the forced current I. This is in contrast to the other structures with symmetric δ for back and front metals, where R_k was not direction dependent (Fig. 5). It is noteworthy that (4) is derived for extracting specific *metal-to-silicon* contact resistance, when only R_{sh} and δ of the diffusion layer are considered, since R_{sh} of the metal is much lower than that of even highly doped silicon. While measuring contact resistance between two materials with similar R_{sh}, δ and R_{sh} of both layers must be taken into account. Therefore, the R_k dependences on δ_B and δ_F were studied separately (Fig. 6a and 6b). It was demonstrated that R_k values increased with increasing δ_B or δ_F.

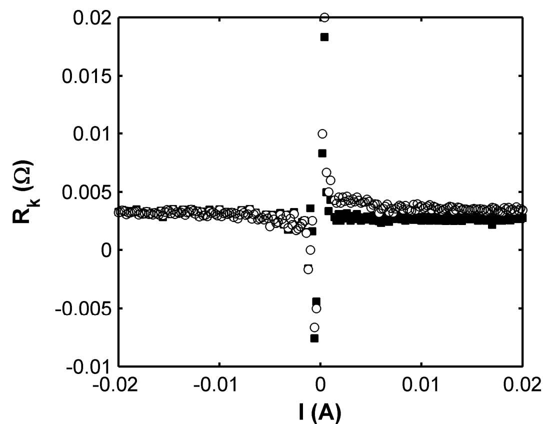

Fig. 5. Measured Kelvin resistance vs. forced current for symmetric (■) (i.e., δ_B=δ_F) and non-symmetric (i.e., $\delta_B \neq \delta_F$) (○) overlaps of square contacts.

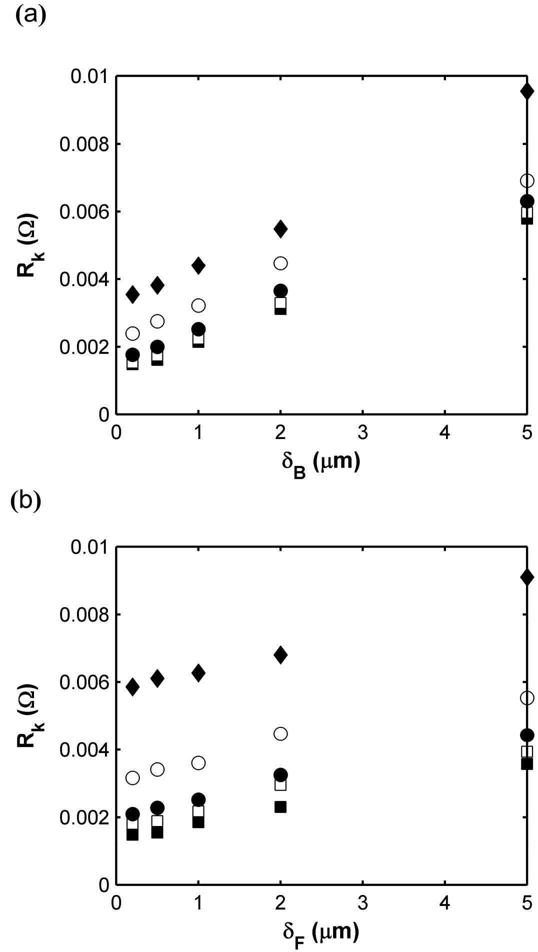

Fig. 6. Dependence of measured Kelvin resistance on overlap size δ_B **(a)** varying δ_F of 0.2 µm (■), 0.5 µm (□),1 µm (●), 2 µm (○), 5 µm (◆) and on overlap size δ_F; **(b)** varying δ_B of 0.2 µm (■), 0.5 µm (□),1 µm (●), 2 µm (○), 5 µm (◆) for given square contact size (L = 8.9 µm).

C. Measured Kelvin resistance R_k for round contacts

For round structures, the R_k data for different metal tap widths (V_{tap}) as a function of contact size *(A)* and overlap size (δ) are given in Fig. 7 and Fig. 8, respectively.

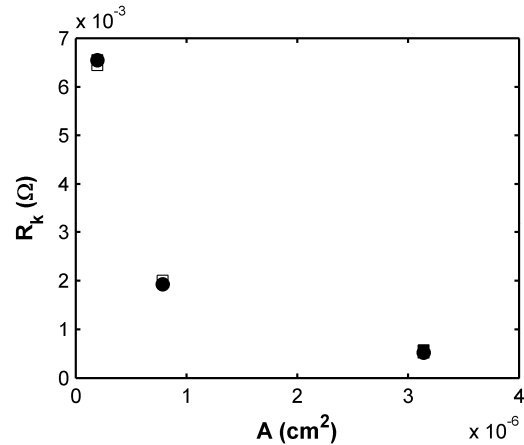

Fig. 7. Measured Kelvin resistance vs. contact size for given symmetric overlap area sizes for round contacts and various V_{tap} = 2 µm (■), V_{tap} = 1.5 µm (□), V_{tap} = 1 µm (●).

Similar to the square contacts, the R_k increased with increasing δ and decreased with increasing A, in agreement with the theory (4). The R_k was not dependent on V_{tap} (Fig. 7 and Fig. 8), proving validity of the measurements and supporting a correct definition of overlap size for round contacts. The R_k behavior for the non-symmetric overlaps was studied by varying δ_B and δ_F separately and revealed the same behavior as for the square contacts.

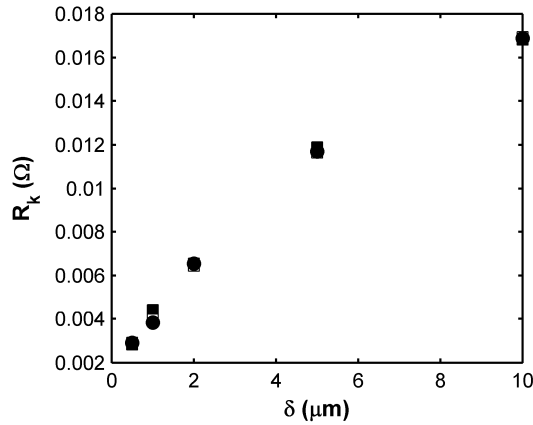

Fig. 8. Measured Kelvin resistance vs. symmetric overlap size for given round contact sizes and various V_{tap} = 2 µm (■), V_{tap} = 1.5 µm (□), V_{tap} = 1 µm (●).

D. Extraction of ρ_c using the analytical model of Schreyer and Saraswat

The specific contact resistance was extracted using both the 1D- and 2D- approximations for a variety of different contact and overlap sizes. The ρ_c values for square contacts with symmetric overlaps can be found in Fig. 9 and Fig. 10. The ρ_c values obtained using the 1D-approach (Fig. 9) were strongly dependent on the contact and overlap size. This supported the significance of applying the 2D-Model instead of the simple 1D-approximation, discussed earlier. The ρ_c values, extracted using the 2D-Model for the smallest contact sizes, were hardly dependent on the overlap dimensions and revealed similar values for different contact sizes. As the contact size increased, the disagreement with the model appeared, showing difference between the geometrical factor, calculated from (4) and the actual geometrical factor, which led to a clear dependence on δ (Fig. 10). For structures with non-symmetrical overlaps, the ρ_c values were extracted by varying δ_B and δ_F separately, using R_{sh} (4) of the corresponding metal layers. An example for δ_B can be found in Fig. 11, where the current direction was from the back to front metal. If the current direction is changed, the ρ_c extracted using δ_F (instead of δ_B) revealed the same values. In summary, it was found that ρ_c is determined by δ_B, if current enters from the back metal and by δ_F if the incoming current is from the front metal.

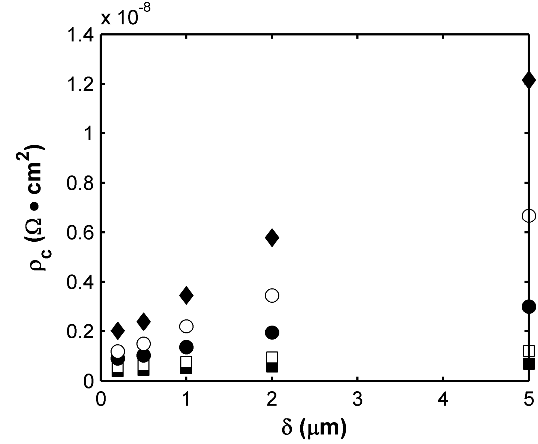

Fig. 9. Specific contact resistance obtained using 1D-approach vs. overlap size for given square contact sizes: L = 1 µm (■), L = 2 µm (□), L = 4.4 µm (●), L = 8.9 µm (○), L = 17.7 µm (◆).

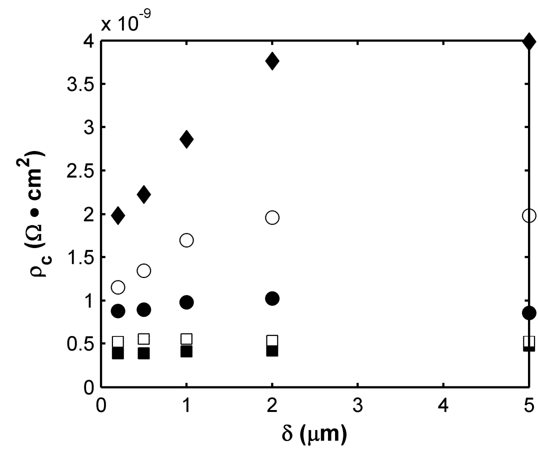

Fig. 10. Specific contact resistance obtained using 2D-approach vs. overlap size for given square contact sizes: L = 1 µm (■), L = 2 µm (□), L = 4.4 µm (●), L = 8.9 µm (○), L = 17.7 µm (◆).

For a given contact size, the ρ_c values obtained using the 1D-approach were also strongly dependent on the overlap size, in contrast to the values, extracted using the 2D-Model (Fig. 11). The latter was also observed for the round contacts with various V_{taps} (Fig. 12).

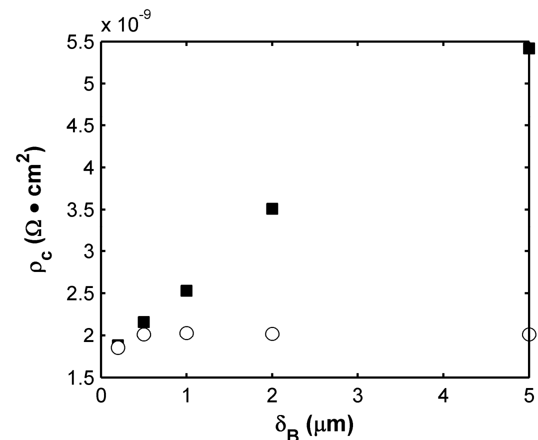

Fig. 11. Specific contact resistance obtained using 1D- (■) and 2D- (○) approach vs. δ_B for given δ_F = 2 µm and square contact size (L = 8.9 µm).

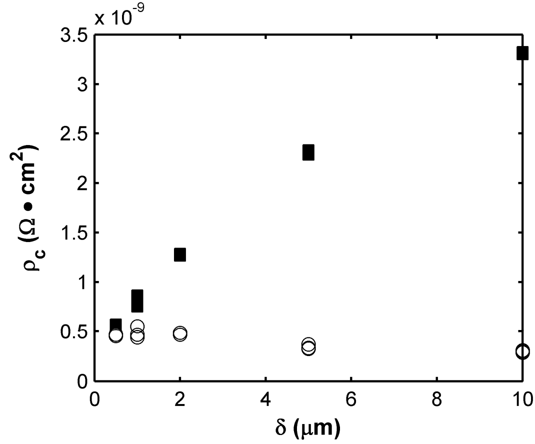

Fig. 12. Specific contact resistance obtained using 1D- (■) and 2D- (○) approach vs. overlap size for given round contact size.

E. Our approach to account for the actual current flow regions

A more accurate approach to extract the ρ_c value is the extrapolation of the measured dependence R_k versus δ to $\delta = 0$, and the calculation of ρ_c from (2) using the R_k value at $\delta = 0$ as the R_c. In this manner the model simplifications, assumed while deriving equation (4), can be ignored. However, for large contacts, the results were still dependent on the contact size (Fig. 13). An explanation of this observation is that the current, which contributes to V_{34}, can flow across a smaller area compared to the actual contact area A. As the contact size becomes larger, this effect enhances, causing significant differences while extracting ρ_c. To account for this effect, the potential distributions along 2 horizontal resistive layers, vertically separated by a resistive "contact", must be considered [10]. For the given test structures, such distributions can be described by the following pair of coupled differential equations:

$$\frac{\partial^2 V_B(x)}{\partial x^2} = \frac{R_{shB}}{\rho_{CG}}\left(V_B(x) - V_F(x)\right) \qquad (5)$$

$$\frac{\partial^2 V_F(x)}{\partial x^2} = \frac{R_{shF}}{\rho_{CG}}\left(V_F(x) - V_B(x)\right), \qquad (6)$$

where V_F(x) and V_B(x) are the potential distributions in the front and back metal layers, respectively, x is the coordinate along the contact length L, R_{shF} and R_{shB} are the sheet resistances of the front and back metals, respectively, and ρ_{CG} corresponds to the specific resistance caused by the properties and geometry of the contact. Applying the boundary conditions, appropriate for the particular geometry, and using ρ_c as a fitting parameter to obtain the corresponding R_k, the $V_{34}(x) = V_F(x) - V_B(x)$ (i.e., voltage difference distribution along the contact) can be calculated. It is important to note that the $V_{34}(x)$ dependence will indicate the actual current flow areas because the current can only flow from the back metal layer into

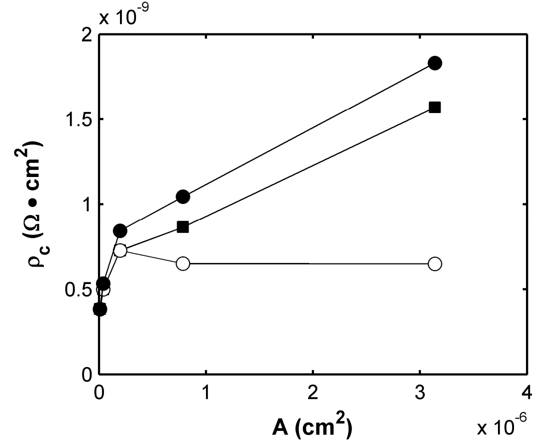

Fig. 13. Specific contact resistance vs. contact size obtained using Schreyer and Saraswat model and then extrapolated to $\delta = 0$ (●), the extrapolation of R_k to $\delta = 0$ (■) and the current-flow area correction (○).

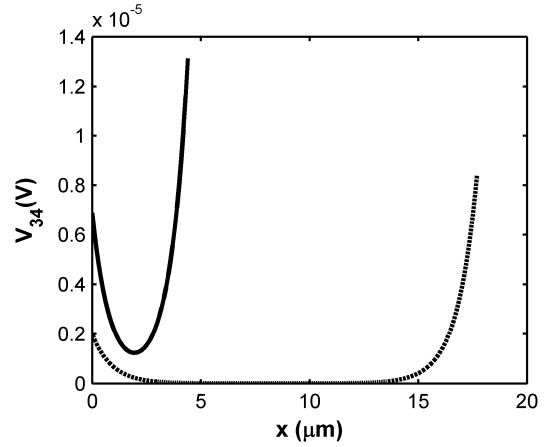

Fig. 14. Potential difference distribution $V_{34}(x) = V_F(x) - V_B(x)$ along the contact coordinate x for the contact length of 4.43 μm (solid line) and 17.72 μm (dashed line).

the front metal layer if $V_{34}(x) \neq 0$. It was shown that for the small contacts, the current flow area was identical to that of the contact, while for the larger contacts this area was much smaller than the designed contact area (Fig. 14). The demonstrated approach allowed to estimate the actual current-flow area size A_{cor} ($A_{cor} < A$) and therefore resulted in a corrected ρ_c. A comparison of the extraction methods is presented in Fig. 13. Our approach results in similar ρ_c values for various contact sizes. This obviously points to the importance of knowing the actual current flow distribution. The extracted ρ_c values were $(6.31 \pm 0.66) \cdot 10^{-10}\ \Omega \cdot cm^2$.

The sheet resistances of both the back and front metal layers were measured using Van-der-Pauw structures, fabricated on the same wafers. The obtained values of 0.054 and 0.027 Ω/□ for the 0.675 μm-thick and 1.4 μm-thick metals, respectively, were in agreement with the corresponding thicknesses. Due to the fact that the two metals had different thicknesses, the potential distribution along the contact was non-symmetrical (Fig. 14). The estimated Kelvin resistance, determined by the two-metal stack of the

known geometry and the sheet resistances, matched with the measured R_k values, thus providing the minimum value of ρ_c to be accurately extracted from these CBKR structures.

CONCLUSIONS

A design and fabrication of various metal-to-metal CBKR structures has been realized. The structures included a large variety of contact geometries, i.e., various shapes and sizes for contact holes and overlap regions. The obtained Kelvin resistance, R_k, was in agreement with the analytical model proposed by Schreyer and Saraswat. This demonstrated the necessity to account for 2D current flow effects around the contact area while measuring low contact resistance values. However, as the calculated ρ_c values were still dependent on the contact size, we developed a new correction method to account for the actual current-flow areas through the contact. The approach allowed to obtain a potential difference distribution along the contact length and led to a physically-correct extraction of the ρ_c. The measured R_k values corresponded to the two-metal stack resistance, calculated from the given dimensions of the contact size and sheet resistances of the metals used. As a result, the minimum value to be accurately extracted from the CBKR structures was determined.

ACKNOWLEDGEMENTS

The authors would like to thank the DIMES Clean room staff of Delft University of Technology for processing the wafers.

REFERENCES

[1] S. Wolf and R. N. Tauber, Silicon Processing for the VLSI Era, ed., vol. 2. Sunset Beach: Lattice Press, 1990.

[2] D. K. Schroder, Semiconductor Material and Device Characterization, 3rd ed. New York: Wiley-Interscience/IEEE, 2006.

[3] W. M. Loh, S. E. Swirhun, E. Crabbe, K. Saraswat, and R. M. Swanson, "An Accurate Method to Extract Specific Contact Resistivity Using Cross-Bridge Kelvin Resistors," IEEE Electron Device Lett., vol. 6, pp. 441-443, 1985.

[4] T. A. Schreyer and K. C. Saraswat, "A Two-Dimensional Analytical Model of the Cross-Bridge Kelvin Resistor," IEEE Electron Device Lett., vol. 7, pp. 661-663, Dec. 1986.

[5] J. Santander, M. Lozano, A. Collado, M. Ullan, and E. Cabruja, "Accurate contact resistivity extraction on Kelvin structures with upper and lower resistive layers," IEEE Trans. Electron Devices, vol. 47, pp. 1431-1439, Jul. 2000.

[6] A. S. Holland, G. K. Reeves, and P. W. Leech, "Universal error corrections for finite semiconductor resistivity in Cross-Kelvin resistor test structures," IEEE Trans. Electron Devices, vol. 51, pp. 914-919, Jun. 2004.

[7] R. L. Gillenwater, M. J. Hafich, and G. Y. Robinson, "Extraction of the Minimum Specific Contact Resistivity Using Kelvin Resistors," IEEE Electron Device Lett., vol. 7, pp. 674-676, Dec. 1986.

[8] M. Finetti, A. Scorzoni, and G. Soncini, "Lateral Current Crowding Effects on Contact Resistance Measurements in 4 Terminal Resistor Test Patterns," IEEE Electron Device Lett., vol. 5, pp. 524-526, 1984.

[9] A. Scorzoni, M. Finetti, K. Grahn, I. Suni, and P. Cappelletti, "Current Crowding and Misalignment Effects as Sources of Error in Contact Resistivity Measurements. 1. Computer-Simulation of Conventional CER and CKR Structures," IEEE Trans. Electron Devices, vol. 34, pp. 525-531, Mar. 1987.

[10] D. B. Scott, W. R. Hunter, and H. Schichijo, "A Transmission-Line Model for Silicided Diffusions - Impact on the Performance of VLSI Circuits," IEEE Trans. Electron Devices, vol. 29, pp. 651-661, 1982.